Exotic Spin Excitations in a Polar Magnet VOSe₂O₅

Tomonao Araki, ^{1,*} Rina Takagi, ^{1,2,‡} Takashi Kurumaji ^{0,3} Yoshinori Tokura ^{0,1,4,5} Masahito Mochizuki, and Shinichiro Seki, and Shinichiro Seki

¹Department of Applied Physics and Institute of Engineering Innovation, University of Tokyo, Tokyo 113-8656, Japan ²PRESTO, Japan Science and Technology Agency (JST), Kawaguchi 332-0012, Japan ³Division of Physics, Mathematics and Astronomy, California Institute of Technology, Pasadena, California 91125, USA ⁴RIKEN Center for Emergent Matter Science (CEMS), Wako 351-0198, Japan

⁵Tokyo College, University of Tokyo, Tokyo 113-8656, Japan ⁶Department of Applied Physics, Waseda University, Tokyo 169-8555, Japan

(Received 14 May 2024; revised 18 July 2024; accepted 22 August 2024; published 24 September 2024)

Magnetic resonance dynamics has been studied for a polar magnet VOSe₂O₅, which hosts several nontrivial magnetic phases including Néel-type skyrmion lattice (SkL). In both cycloidal and SkL spin states, two excitation modes active to oscillating magnetic field $B_{\nu} \perp c$ and one mode active to $B_{\nu} \parallel c$ are identified. The subsequent micromagnetic simulations well reproduce the observed selection rules and relative resonance frequencies, which allows the unambiguous assignment of the spin oscillation manner for each mode. Interestingly, the IC-2 phase with a potential double-q character was found to host similar excitation modes as the SkL state. We also discovered the existence of the novel B' phase with four modes active to $B_{\nu} \perp c$. The present results provide a fundamental basis for the comprehensive understanding of resonant spin dynamics in polar magnets, and highlight VOSe₂O₅ as a unique material platform to host a rich variety of nontrivial spin excitations.

DOI: 10.1103/PhysRevLett.133.136702

Recently, exotic spin textures emerging in noncentrosymmetric systems are attracting much attention. Typical examples are magnetic skyrmions [i.e., a topologically stable swirling spin texture with particlelike character as shown in Fig. 1(c)] [1–3] and chiral magnetic soliton [4,5], both of which have been intensively studied as a potential candidate of unique information medium. Dynamics of such modulated spin textures often serves as a source of rich emergent phenomena [6–11], and the comprehensive understanding and exploration of novel magnetic systems to host unconventional spin excitation is an important challenge.

In noncentrosymmetric systems, the spin swirling manner is generally governed by the symmetry of underlying crystal lattice and associated Dzyaloshinskii-Moriya (DM) interaction [3,12–14]. In the case of the polar (chiral) system, the DM interaction favors the cycloidal (screw) spin texture in the zero-field ground state, where neighboring spins rotate within a plane parallel (normal) to the magnetic modulation vector q. By applying static magnetic field B_0 , triangular lattice of Néel-type (Bloch-type) skyrmion is stabilized, which can be considered as a kind of triple-q order, i.e., the superposition of three cycloidal (screw) spin orders with different q vectors [15,16].

Magnetic skyrmions were originally discovered in a series of chiral cubic systems, such as B20 alloys [15,17] and Cu₂OSeO₃ [18]. The associated magnetic resonance experiments clarified the excitation modes in both screw and Bloch-type skyrmion lattice (SkL) states [7,19–24], the latter of which hosts three excitation modes corresponding to the counterclockwise (CCW), clockwise (CW), and breathing (BR) oscillation of skyrmion core.

On the other hand, still less explored is the spin dynamics in the polar systems. In bulk compounds, the first observation of Néel-type skyrmion was reported for a lacunar spinel GaV₄S₈ [16,25–29]. Nevertheless, this compound has a nonpolar cubic structure at room temperature, and the polar rhombohedral structure is stabilized only below 42 K. In the latter polar phase, the original cubic lattice is stretched along one of four cubic (111) axes, which inevitably leads to the coexistence of multiple structural domains with different orientations of polar axes. Such a multidomain character prevented the detailed analysis of resonant spin dynamics in GaV₄S₈ [30,31]. At this stage, the full identification of the selection rule and spin oscillation manner for each excitation mode (including the one for the cycloidal spin states), as well as the quantitative explanation of observed spectra based on the microscopic Hamiltonian, are yet to be achieved. For a better understanding of magnetic resonance spectra in the polar system, the employment of appropriate materials with a single polar domain is essential.

^{*}Contact author: araki@topo.t.u-tokyo.ac.jp

^{*}Contact author: seki@ap.t.u-tokyo.ac.jp

^{*}Present address: The Institute for Solid State Physics, University of Tokyo, Kashiwa 277-8581, Japan.

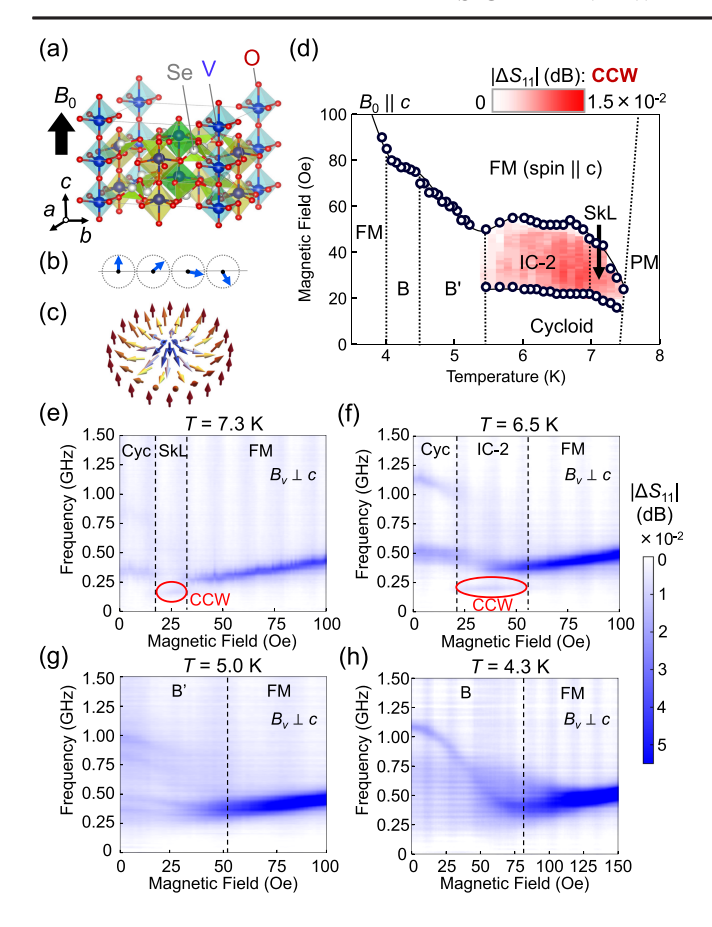


FIG. 1. (a) Crystal structure of $VOSe_2O_5$. (b),(c) Schematic of cycloidal and Néel-type skyrmion spin textures. (d) B_0 -T phase diagram for $B_0 \parallel c$ determined by magnetic resonance measurements. The background color represents the amplitude of microwave absorption $|\Delta S_{11}|$ by the CCW(-like) mode. (e)–(h) B_0 ($\parallel c$)-dependence of microwave absorption spectra measured for the $B_{\nu} \perp c$ configuration, where the color represents the microwave absorption amplitude $|\Delta S_{11}|$. In (e) and (f), CCW(-like) mode is highlighted by ellipses. Cyc, SkL, FM and PM represent the cycloidal, skyrmion lattice, ferromagnetic and paramagnetic phases, respectively.

Our target material VOSe₂O₅ is known as another example of polar skyrmion-hosting magnet [32,33]. It is characterized by the tetragonal crystal structure belonging to a polar space group P4cc as shown in Fig. 1(a) [34–36]. Notably, this polar structure is stable from its growth temperature, and therefore the crystal retains the single polar domain state. The magnetism is governed by V^{4+} (S = 1/2) ions, which form square lattices stacked along the c axis (i.e., polar axis). Figure 1(d) summarizes the B_0 -T (temperature) magnetic phase diagram of VOSe₂O₅ for $B_0 \| c$. At temperature just below $T_c \sim 8$ K, DM interaction stabilizes the cycloidal spin order [Fig. 1(b)] with magnetic modulation vector $q||\langle 100 \rangle|$ at $B_0 = 0$, as well as the triangular lattice of Néel-type skyrmions [Fig. 1(c)] under $B_0 || c$. At lower temperatures, the appearance of more exotic magnetic phases (IC-2 and B) was also reported [Fig. 1(d)], and this compound can be considered as an ideal model system for the systematic investigation of resonant spin dynamics under the polar environment. In this Letter, we intensively studied the magnetic resonance spectra for VOSe₂O₅ to obtain a comprehensive understanding of spin dynamics in polar systems and explore a rich variety of nontrivial spin excitations.

Single crystals of VOSe₂O₅ were grown by chemical vapor transport methods [32]. Microwave absorption spectra $\Delta S_{11}(\nu)$ associated with magnetic resonance is measured by a vector network analyzer [20,22]. A microstripline was used to apply an oscillating magnetic field B_{ν} of microwave to the sample (Fig. S1), which was located in a cryostat equipped with a superconducting magnet [37].

Figure 2(a) indicates B_0 dependence of magnetization Mand $\partial M/\partial B_0$ measured for $B_0||c$ at 7.3 K. According to the previous studies [32,33], the cycloidal magnetic order [Fig. 1 (b)] is realized in the zero-field ground state. By increasing the amplitude of B_0 , the $\partial M/\partial B_0$ profile shows a clear dip structure for 15 Oe $< B_0 <$ 30 Oe, which signals the appearance of the SkL state. In the higher B_0 region, the saturated ferromagnetic state is realized. The corresponding B_0 dependence of microwave absorption spectra measured for the microwave polarizations $B_{\nu} \perp c$ and $B_{\nu} \parallel c$ is summarized in Figs. 2(b) and 2(c), respectively. Here, the background color indicates the amplitude of microwave absorption $|\Delta S_{11}|$, and the $\Delta S_{11}(\nu)$ spectra measured for various B_0 values are shown in Fig. 2(d). In the cycloidal magnetic phase, two magnetic resonance modes are identified at around 0.4 and 0.8 GHz for $B_{\nu} \perp c$, and another mode is observed at 0.2 GHz for $B_{\nu} \parallel c$. In the SkL state, there are two resonance modes at 0.3 GHz and 0.2 GHz for $B_{\nu} \perp c$ and another mode at 0.1 GHz for $B_{\nu} \parallel c$. In contrast, the ferromagnetic state hosts only a single excitation mode for $B_{\nu} \perp c$, which corresponds to a conventional Kittel mode with B_0 -linear frequency. Experimentally observed B_0 dependence of resonance frequency for each excitation mode is summarized in Fig. 3(b).

Next, for microscopic clarifications of the excitation modes, we performed micromagnetic simulations of spin dynamics using the Landau-Lifshitz-Gilbert equation [19]. To consider the polar tetragonal crystal symmetry and the weak easy-axis magnetic anisotropy of VOSe₂O₅, we employed a classical Heisenberg model on stacked square lattices whose Hamiltonian is given by

$$\mathcal{H} = -J_{xy} \sum_{\langle i,j \rangle}^{xy} \left[m_i^x m_j^x + m_i^y m_j^y + (1+\Delta) m_i^z m_j^z \right]$$

$$-J_z \sum_{i}^{z} \boldsymbol{m}_i \cdot \boldsymbol{m}_{i+\hat{z}} - B_0' \sum_{i} m_i^z$$

$$-D \sum_{i} \left[(\boldsymbol{m}_i \times \boldsymbol{m}_{i+\hat{x}}) \times \hat{y} - (\boldsymbol{m}_i \times \boldsymbol{m}_{i+\hat{y}}) \times \hat{x} \right], \qquad (1)$$

where $\mathbf{m}_i = (m_i^x, m_i^y, m_i^z)$ is the normalized classical spin vectors on the *i*th site, and \hat{x} , \hat{y} , and \hat{z} are the unit directional

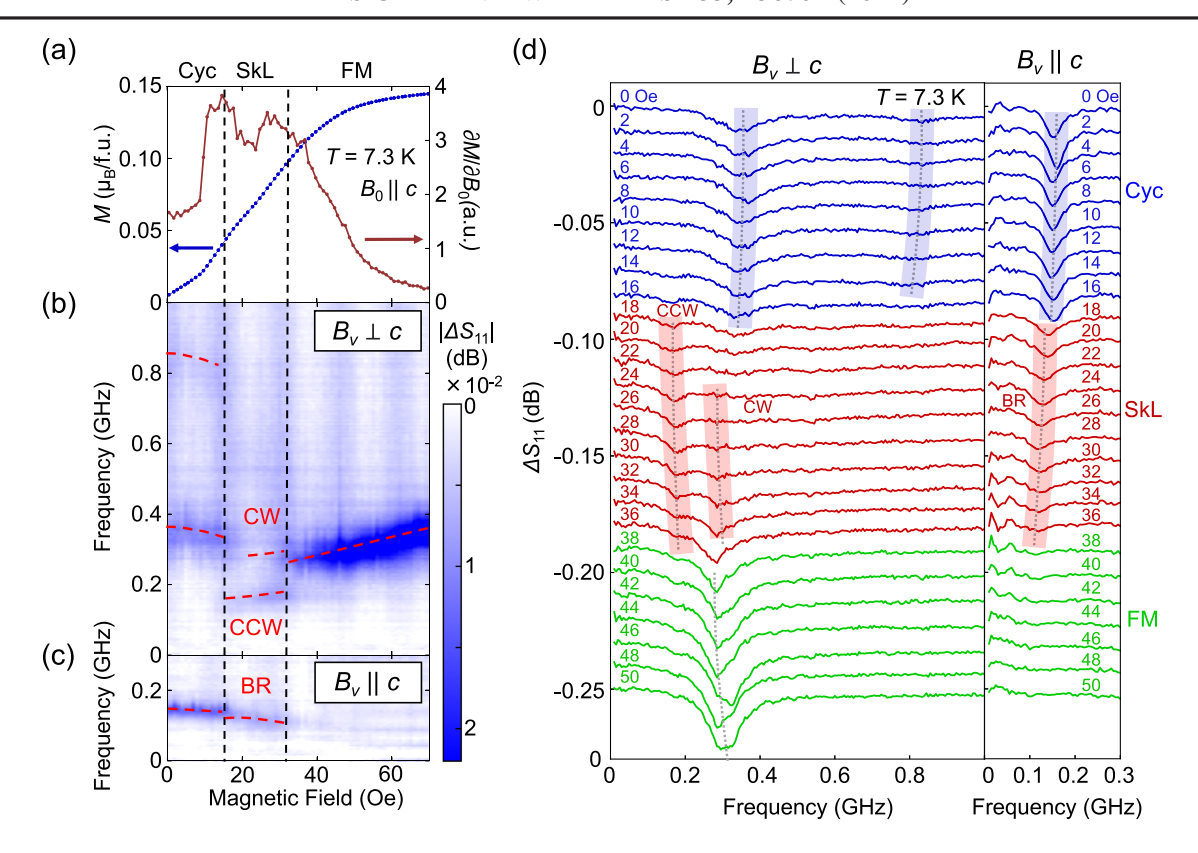


FIG. 2. (a)–(c) Magnetic field dependence of magnetization M and $\partial M/\partial B_0$ (a) and microwave absorption spectra for the microwave polarizations $B_{\nu} \perp c$ (b) and $B_{\nu} \parallel c$ (c) measured at 7.3 K for $B_0 \parallel c$. In (b) and (c), the color represents the amplitude of microwave absorption $|\Delta S_{11}|$. (d) Microwave absorption spectra measured at various amplitudes of $B_0 \parallel c$, with the microwave polarizations $B_{\nu} \perp c$ (left panel) and $B_{\nu} \parallel c$ (right panel). Data are shifted along the vertical direction for clarity. In (b)–(d), the frequency of magnetic resonance modes is highlighted by dashed lines.

vectors. The first and second terms represent the intraplane and interplane exchange interactions where $\Delta(>0)$ represents the strength of XXZ-type easy-axis anisotropy. The third term depicts the Zeeman interactions associated with the static magnetic field $\boldsymbol{B}_0 = (0,0,B_0)$ applied along the c axis, where we defined $B'_0 = g\mu_{\rm B}SB_0$. g is the g factor, $\mu_{\rm B}$ is the Bohr magneton, and S is the value of spin. The fourth term represents the DM interaction. The summation $\sum_{\langle i,j\rangle}$ is taken over the nearest-neighbor site pairs. Unless specified, we adopted the parameter values of $J_{xy} = J_z = J = 1$, D = 0.18, and $\Delta/J = 0.02$ and the system size of $144 \times 144 \times 6$ sites [37].

Figure 3(a) shows the calculated magnetic field dependence of magnetic resonance frequency for the microwave polarizations $B_{\nu}\bot c$ (upper panel) and $B_{\nu}\|c$ (lower panel). In both cycloidal and Néel-type SkL phases, two resonance modes are identified for $B_{\nu}\bot c$ and one resonance mode for $B_{\nu}\|c$. These theoretical results reproduce well the experimental results at 7.3 K in Fig. 3(b) with respect to the number of excitation modes and their relative frequencies for both microwave polarizations.

By analyzing the temporal evolutions of spin configurations, the spin oscillation manners in respective excitation modes were further identified as illustrated in Figs. 3(c)–3(h). In the cycloidal spin state, there appear three excitation modes active, respectively, to $B_{\nu}\|b$, $B_{\nu}\|a$, and $B_{\nu}\|c$ in the descending order from higher to lower frequencies, in which the local magnetizations rotate around the b, a, and c axes, respectively. Here, the b axis is defined to be parallel to the magnetic modulation vector q. The mode active to $B_{\nu}\|a$ is the phason mode [Fig. 3(d)], while the mode active to $B_{\nu}\|b$ corresponds to the oscillatory rotation of spin-spiral plane around the q vector or the b axis [Fig. 3(c)]. In the SkL state, the lower- and higher-frequency modes active to $B_{\nu}\perp c$ are the CCW and CW rotation modes [Figs. 3(f) and 3(g)], respectively, while the mode active to $B_{\nu}\|c$ is the BR mode [Fig. 3(h)].

Compared with the typical skyrmion-hosting materials with chiral cubic crystal structures [21], VOSe₂O₅ with a polar crystal structure has several unique features. In chiral cubic systems, the single-q screw magnetic order at $B_0=0$ hosts only two excitation modes with nearly the same frequencies, and the frequency of the BR mode is located between those of CW and CCW modes in the SkL state. In the case of polar VOSe₂O₅, by contrast, the single-q cycloidal spin state at $B_0=0$ hosts three excitation modes, and the BR mode in the SkL state is located below the CW and CCW modes in frequency.

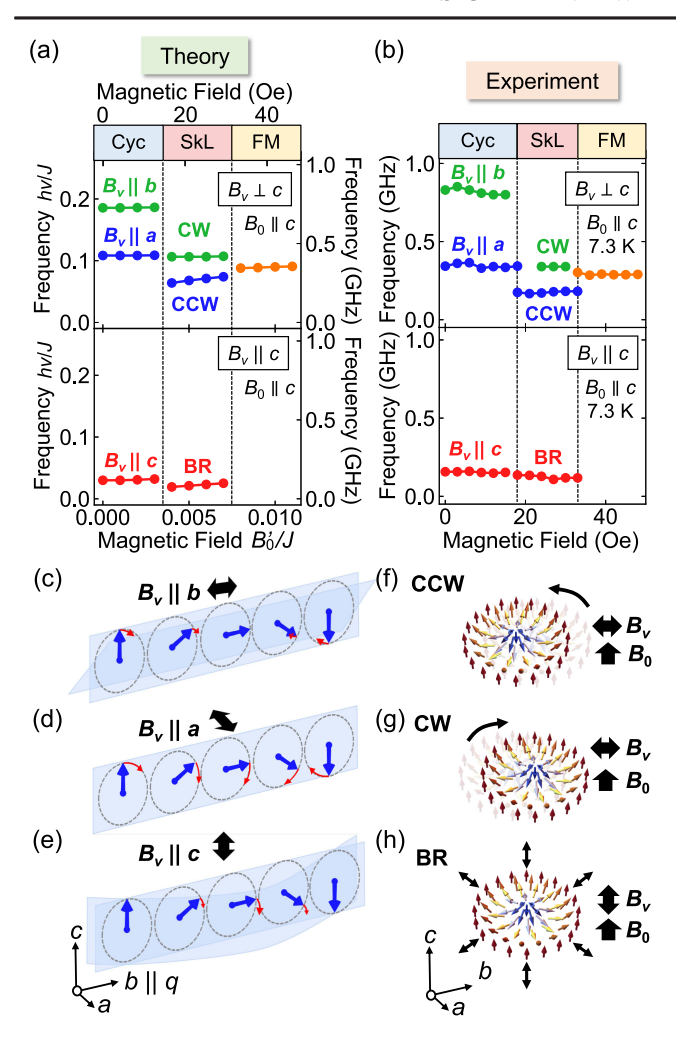


FIG. 3. Magnetic field dependence of magnetic resonance frequency (a) theoretically calculated with $\Delta/J=0.02$ and (b) experimentally observed at 7.3 K. In (a), the vertical axis on the right side and the upper horizontal axis indicate the frequency and magnetic field values calculated by assuming $J=1.8\times 10^{-2}$ meV and $g\mu_{\rm B}S=2.4\times 10^{-2}$ meV/T, respectively. (c)–(e) Schematic of magnetic resonance modes active to $B_{\nu}\|b(\|q),\ B_{\nu}\|a(\perp q),$ and $B_{\nu}\|c$ in the cycloidal spin state, in which magnetic moments temporally rotate around the $b(\|q),\ a(\perp q),\ and\ c$ axes, respectively. (f)–(h) Schematic of counterclockwise (CCW) and clockwise (CW) rotation modes active to $B_{\nu}\perp c$, and breathing (BR) mode active to $B_{\nu}\parallel c$, in the Néel-type SkL state.

To investigate the origin of such differences, we calculated the Δ dependence of resonance frequency and the absorption intensity for each excitation mode as summarized in Fig. 4. In the cycloidal spin state with $\Delta=0$, which corresponds to the isotropic cubic limit, the mode in Fig. 3(c) is not active to $B_{\nu}\|b$, and only two resonance modes active respectively to $B_{\nu}\|a$ and $B_{\nu}\|c$ with nearly the same frequencies are observed. On the contrary, the mode in Fig. 3(c) becomes active to $B_{\nu}\|b$ when $\Delta>0$, which indicates that the easy-axis anisotropy is essential for the

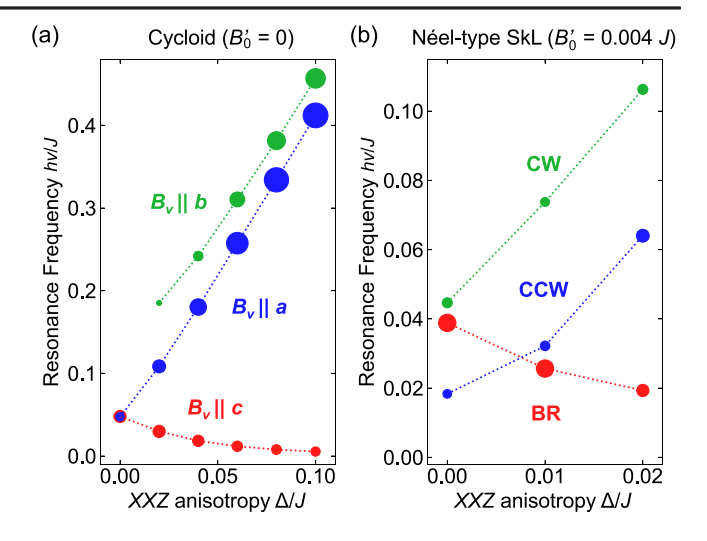


FIG. 4. Calculated resonance frequencies for the (a) cycloidal and (b) Néel-type SkL states as functions of easy-axis exchange anisotropy Δ . The size of data points scales with the absorption strength for each mode (see Fig. S6 [37]).

appearance of three resonance modes in the cycloidal spin state. Here, the introduction of $\Delta > 0$ also leads to the decrease (increase) of resonance frequency for $B_{\nu} || c (B_{\nu} || b)$ and $B_{\nu}||a\rangle$. In the SkL state, the frequency of the BR mode is located between the CW and CCW modes for $\Delta = 0$, while the frequency decreases (increases) for the BR mode (CW and CCW modes) when $\Delta > 0$. In general, the mode active to $B_{\nu} \| c (B_{\nu} \perp c)$ is characterized by the oscillation of net magnetization along the direction parallel (normal) to the c axis. The introduction of easy-axis anisotropy reduces (enhances) the energy cost required for such excitations, which well accounts for the theoretical Δ dependence of the resonance frequency. From the comparison with experimental data in Fig. 3(b), we concluded that the experimental magnetic resonance spectra at 7.3 K are well reproduced for $\Delta/J \sim 0.02$.

Figures 1(f)-1(h) indicate the B_0 dependence of magnetic resonance spectra experimentally measured for $B_{\nu} \perp c$ at 6.5 K, 5.0 K, and 4.3 K. At 6.5 K [Fig. 1(f)], the low-field cycloidal spin state hosts the same modes as observed at 7.3 K [Figs. 1(e) and 2(b)]. In the field-induced IC-2 state, we observed excitation modes similar to those in the SkL state, in particular, the CCW-like mode at ~ 0.2 GHz. In the B_0 -T phase diagram in Fig. 1(d), the amplitude $|\Delta S_{11}|$ of the CCW(-like) mode is plotted as background colors, which shows that this mode commonly appears in the SkL and IC-2 phases. For the IC-2 phase, the previous neutron scattering experiments suggested the potential realization of anisotropic double-q magnetic order with a vortexlike arrangement of in-plane spin component [32,33,38]. Since the rotational oscillation of the spin-vortex core is allowed only in the multi-q states, the present observation of the CCW-like mode suggests the validity of such a double-q picture in the IC-2 phase.

In the temperature region 4.5 K < T < 5.4 K, we discovered the appearance of the novel B' phase, which was not previously identified [Fig. 1(d)]. The spectra in the B' phase resemble those in the cycloidal phase, but the original two excitation modes split into four modes [Figs. 1(g) and S3(b)]. In the B phase ranging in 4.0 K < T < 4.5 K, these modes disappear and another new excitation mode emerges [Fig. 1(h)]. Below 4.0 K, the sign of magnetic anisotropy is reversed, and the easy-plane ferromagnetic order with a broad magnetic resonance peak is stabilized (Fig. S4) [37].

In VOSe₂O₅, the amplitude and sign of exchange anisotropy Δ , as well as the relative amplitude of other competing higher-order interactions neglected in Eq. (1), are expected to change as a function of temperature [32]. Our present results suggest that such a delicate balance of magnetic interactions causes an exceptionally rich variety of exotic magnetic phases and associated collective excitation dynamics in this compound. Further investigation of the detailed magnetic structure in the IC-2, B', and B phases, as well as their formation mechanism and character of excitation modes, will be interesting for future study [37].

In summary, we systematically investigated the magnetic resonance spectra for VOSe₂O₅ characterized by the single polar domain. In both cycloidal and Néel-type SkL spin states, two modes active to $B_{\nu} \perp c$ and one mode active to $B_{\nu}||c|$ are identified. The subsequent micromagnetic simulations reproduce well the observed selection rules and the relative resonance frequencies, which allows the unambiguous assignment of the spin oscillation manner for each mode. Notably, the IC-2 phase with a potential double-q character is found to host similar excitation modes as the triangular SkL state. We also discovered the existence of a novel B' phase with four modes active to $B_{\nu} \perp c$. The present results provide a fundamental basis for the comprehensive understanding of resonant spin dynamics in polar magnets, and highlight VOSe₂O₅ as a unique material platform to host a rich variety of nontrivial spin excitations.

Acknowledgments—The authors thank A. Kikkawa and N. D. Khanh for enlightening discussions and experimental help. This work was partly supported by Grants-In-Aid for Scientific Research (Grants No. 18H03685, No. 20H00337, No. 20H00349, No. 21H04440, No. 21H04990, No. 21K13876, No. 21K18595, No. 22H04965, 23H04522, No. 23KJ0664, No. 24H02235, No. 24H02231, No. 24K00579) from JSPS, PRESTO (Grants No. JPMJPR18L5, No. JPMJPR20B4) and CREST (Grants No. JPMJCR1874, No. JPMJCR20T1, No. JPMJCR23O4) from JST, Katsu Research Encouragement Award and UTEC-UTokyo FSI Research Grant Program of the University of Tokyo, Asahi Glass Foundation, Murata Science Foundation and Foundation for Promotion of Material Science and Technology of Japan (MST Foundation). T. A. thanks the World-leading Innovative Graduate Study Program for Materials Research, Information, and Technology (MERIT-WINGS). M. M. thanks Waseda University Grant for Special Research Projects (Grant No. 2024C-153). This work was partly performed using the facilities of the Cryogenic Research Center, The University of Tokyo. The illustration of crystal structure was drawn by VESTA [39].

- A. Fert, N. Reyren, and V. Cros, Nat. Rev. Mater. 2, 17031 (2017).
- [2] N. Nagaosa and Y. Tokura, Nat. Nanotechnol. 8, 899 (2013).
- [3] Y. Tokura and N. Kanazawa, Chem. Rev. **121**, 5, 2857 (2021).
- [4] Y. Togawa, T. Koyama, K. Takayanagi, S. Mori, Y. Kousaka, J. Akimitsu, S. Nishihara, K. Inoue, A. S. Ovchinnikov, and J. Kishine, Phys. Rev. Lett. 108, 107202 (2012).
- [5] Y. Shimamoto, Y. Matsushima, T. Hasegawa, Y. Kousaka, I. Proskurin, J. Kishine, A. S. Ovchinnikov, F. J. T. Goncalves, and Y. Togawa, Phys. Rev. Lett. 128, 247203 (2022).
- [6] T. Weber et al., Science 375, 1025 (2022).
- [7] M. Garst, J. Waizner, and D. Grundler, J. Phys. D 50, 293002 (2017).
- [8] T. Yokouchi, F. Kagawa, M. Hirschberger, Y. Otani, N. Nagaosa, and Y. Tokura, Nature (London) 586, 232 (2020).
- [9] K. Tanabe, D. Chiba, J. Ohe, S. Kasai, H. Kohno, S. E. Barnes, S. Maekawa, K. Kobayashi, and T. Ono, Nat. Commun. 3, 845 (2012).
- [10] T. Schulz, R. Ritz, A. Bauer, M. Halder, M. Wagner, C. Franz, C. Pfleiderer, K. Everschor, M. Garst, and A. Rosch, Nat. Phys. 8, 301 (2012).
- [11] S. E. Barnes and S. Maekawa, Phys. Rev. Lett. **98**, 246601 (2007).
- [12] A. Bogdanov and A. Hubert, J. Magn. Magn. Mater. 138, 255 (1994).
- [13] I. Dzyaloshinskii, J. Phys. Chem. Solids 4, 241 (1958).
- [14] T. Moriya, Phys. Rev. 120, 91 (1960).
- [15] S. Mühlbauer, B. Binz, F. Jonietz, C. Pfleiderer, A. Rosch, A. Neubauer, R. Georgii, and P. Böni, Science 323, 915 (2009).
- [16] I. Kézsmárki et al., Nat. Mater. 14, 1116 (2015).
- [17] X. Z. Yu, Y. Onose, N. Kanazawa, J. H. Park, J. H. Han, Y. Matsui, N. Nagaosa, and Y. Tokura, Nature (London) 465, 901 (2010).
- [18] S. Seki, X. Z. Yu, S. Ishiwata, and Y. Tokura, Science 336, 198 (2012).
- [19] M. Mochizuki, Phys. Rev. Lett. 108, 017601 (2012).
- [20] Y. Onose, Y. Okamura, S. Seki, S. Ishiwata, and Y. Tokura, Phys. Rev. Lett. **109**, 037603 (2012).
- [21] T. Schwarze, J. Waizner, M. Garst, A. Bauer, I. Stasinopoulos, H. Berger, C. Pfleiderer, and D. Grundler, Nat. Mater. 14, 478 (2015).
- [22] Y. Okamura, F. Kagawa, M. Mochizuki, M. Kubota, S. Seki, S. Ishiwata, M. Kawasaki, Y. Onose, and Y. Tokura, Nat. Commun. 4, 2391 (2013).
- [23] S. Seki, M. Garst, J. Waizner, R. Takagi, N. D. Khanh, Y. Okamura, K. Kondou, F. Kagawa, Y. Otani, and Y. Tokura, Nat. Commun. 11, 256 (2020).
- [24] M. Mochizuki and S. Seki, J. Phys. Condens. Matter 27, 503001 (2015).

- [25] E. Ruff, S. Widmann, P. Lunkenheimer, V. Tsurkan, S. Bordács, I. Kézsmárki, and A. Loidl, Sci. Adv. 1, e1500916 (2015).
- [26] J. S. White, A. Butykai, R. Cubitt, D. Honecker, C. D. Dewhurst, L. F. Kiss, V. Tsurkan, and S. Bordács, Phys. Rev. B 97, 020401(R) (2018).
- [27] K. Xu and H. J. Xiang, Phys. Rev. B 92, 121112(R) (2015).
- [28] P. Padmanabhan, F. Sekiguchi, R. B. Versteeg, E. Slivina, V. Tsurkan, S. Bordacs, I. Kezsmarki, and P. H. M. vanLoosdrecht, Phys. Rev. Lett. 122, 107203 (2019).
- [29] F. Sekiguchi, K. Budzinauskas, P. Padmanabhan, R. B. Versteeg, V. Tsurkan, I. Kézsmárki, F. Foggetti, S. Artyukhin, and P. H. M. van Loosdrecht, Nat. Commun. 13, 3212 (2022).
- [30] D. Ehlers, I. Stasinopoulos, V. Tsurkan, H. A. KrugvonNidda, T. Feher, A. Leonov, I. Kezsmarki, D. Grundler, and A. Loidl, Phys. Rev. B 94, 014406 (2016).
- [31] Y. Okamura, S. Seki, S. Bordacs, A. Butykai, V. Tsurkan, I. Kezsmarki, and Y. Tokura, Phys. Rev. Lett. 122, 057202 (2019).
- [32] T. Kurumaji, T. Nakajima, V. Ukleev, A. Feoktystov, T. H. Arima, K. Kakurai, and Y. Tokura, Phys. Rev. Lett. 119, 237201 (2017).

- [33] T. Kurumaji, T. Nakajima, A. Feoktystov, E. Babcock, Z. Salhi, V. Ukleev, T.-h. Arima, K. Kakurai, and Y. Tokura, J. Phys. Soc. Jpn. 90, 024705 (2021).
- [34] P. G. Meunier, M. Bertaud, and J. Galy, Acta Crystallogr. Sect. B 30, 2834 (1974).
- [35] J.-C. Trombe, A. Gleizes, J. Galy, J.-P. Renard, Y. Journaux, and M. Verdaguer, Nouveau Journal de chimie 11, 321 (1987).
- [36] S.-H. Kim, P. Shiv Halasyamani, B. C. Melot, R. Seshadri, M. A. Green, A. S. Sefat, and D. Mandrus, Chem. Mater. 22, 5074 (2010).
- [37] See Supplemental Material at http://link.aps.org/supplemental/10.1103/PhysRevLett.133.136702 for the details of experimental methods, measured magnetic resonance spectra, and theoretical simulations. Temperature dependence of magnetic resonance spectra is also provided as Supplemental Videos 1 and 2.
- [38] S. D. Yi, S. Onoda, N. Nagaosa, and J. H. Han, Phys. Rev. B 80, 054416 (2009).
- [39] K. Momma and F. Izumi, J. Appl. Crystallogr. 44, 1272 (2011).